NAVAL POSTGRADUATE SCHOOL

MONTEREY, CALIFORNIA

THESIS

A COMSOL SIMULATION OF MICROSPHERE-BASED PASSIVE MATERIAL FOR LOW TEMPERATURE DIVING SUITS

by

John A. Oldenkamp

September 2018

Thesis Advisor:	Emil P. Kartalov

THIS PAGE INTENTIONALLY LEFT BLANK

REPORT DOCUMENTATION PAGE			*Form Approved OMB No. 0704-0188*
Public reporting burden for this collection of information is estimated to average 1 hour per response, including the time for reviewing instruction, searching existing data sources, gathering and maintaining the data needed, and completing and reviewing the collection of information. Send comments regarding this burden estimate or any other aspect of this collection of information, including suggestions for reducing this burden, to Washington headquarters Services, Directorate for Information Operations and Reports, 1215 Jefferson Davis Highway, Suite 1204, Arlington, VA 22202-4302, and to the Office of Management and Budget, Paperwork Reduction Project (0704-0188) Washington, DC 20503.			
1. AGENCY USE ONLY *(Leave blank)*	**2. REPORT DATE** September 2018	**3. REPORT TYPE AND DATES COVERED** Master's thesis	
4. TITLE AND SUBTITLE A COMSOL SIMULATION OF MICROSPHERE-BASED PASSIVE MATERIAL FOR LOW TEMPERATURE DIVING SUITS			**5. FUNDING NUMBERS**
6. AUTHOR(S) John A. Oldenkamp			
7. PERFORMING ORGANIZATION NAME(S) AND ADDRESS(ES) Naval Postgraduate School Monterey, CA 93943-5000			**8. PERFORMING ORGANIZATION REPORT NUMBER**
9. SPONSORING / MONITORING AGENCY NAME(S) AND ADDRESS(ES) Office of Naval Research, Arlington, VA 22206			**10. SPONSORING / MONITORING AGENCY REPORT NUMBER**
11. SUPPLEMENTARY NOTES The views expressed in this thesis are those of the author and do not reflect the official policy or position of the Department of Defense or the U.S. Government.			
12a. DISTRIBUTION / AVAILABILITY STATEMENT Approved for public release. Distribution is unlimited.			**12b. DISTRIBUTION CODE** A

13. ABSTRACT (maximum 200 words)

The United States Navy conducts diving operations in various places and climates all over the world. The neoprene wet suit protects the diver from cold water temperatures, extending the duration the diver can stay in the water. Neoprene is a soft material made of air-foamed rubber that uses small, flexible air pockets to thermally insulate a diver from the cold. However, as the diver descends, increased ambient pressure compresses the neoprene, decreasing its thickness and shrinking its air pockets. As a result, the suit's insulation capability significantly degrades with depth, adversely affecting diver operations and persistence time at depth. One potential solution is the use of rigid glass microspheres as the thermally insulating material, which should be impervious to pressure changes associated with diving depth. This thesis develops a model using COMSOL Multiphysics software that can be used to theoretically verify previous work and provide the framework for computer simulations to predict the thermal resistivity of various materials as a function of microsphere composition, steric distribution, and volumetric fraction within the carrier polymer.

14. SUBJECT TERMS diver, insulation, thermal, composite, material, microspheres, silicone, protection, divesuit, diving, safety, hypothermia			**15. NUMBER OF PAGES** 71
			16. PRICE CODE
17. SECURITY CLASSIFICATION OF REPORT Unclassified	**18. SECURITY CLASSIFICATION OF THIS PAGE** Unclassified	**19. SECURITY CLASSIFICATION OF ABSTRACT** Unclassified	**20. LIMITATION OF ABSTRACT** UU

THIS PAGE INTENTIONALLY LEFT BLANK

A COMSOL SIMULATION OF MICROSPHERE-BASED PASSIVE MATERIAL FOR LOW TEMPERATURE DIVING SUITS

John A. Oldenkamp
Lieutenant, United States Navy
BS, United States Naval Academy, 2009

Submitted in partial fulfillment of the
requirements for the degree of

MASTER OF SCIENCE IN APPLIED PHYSICS

from the

NAVAL POSTGRADUATE SCHOOL
September 2018

Approved by: Emil P. Kartalov
                 Advisor

                 Kevin B. Smith
                 Chair, Department of Physics

THIS PAGE INTENTIONALLY LEFT BLANK

ABSTRACT

The United States Navy conducts diving operations in various places and climates all over the world. The neoprene wet suit protects the diver from cold water temperatures, extending the duration the diver can stay in the water. Neoprene is a soft material made of air-foamed rubber that uses small, flexible air pockets to thermally insulate a diver from the cold. However, as the diver descends, increased ambient pressure compresses the neoprene, decreasing its thickness and shrinking its air pockets. As a result, the suit's insulation capability significantly degrades with depth, adversely affecting diver operations and persistence time at depth. One potential solution is the use of rigid glass microspheres as the thermally insulating material, which should be impervious to pressure changes associated with diving depth. This thesis develops a model using COMSOL Multiphysics software that can be used to theoretically verify previous work and provide the framework for computer simulations to predict the thermal resistivity of various materials as a function of microsphere composition, steric distribution, and volumetric fraction within the carrier polymer.

THIS PAGE INTENTIONALLY LEFT BLANK

TABLE OF CONTENTS

LIST OF FIGURES

LIST OF TABLES

THIS PAGE INTENTIONALLY LEFT BLANK

LIST OF ACRONYMS AND ABBREVIATIONS

BCC	body centered cubic
FCC	face centered cubic
FSW	feet of seawater
PDMS	polydimethylsiloxane
PSIG	pounds per square inch, gage
SCUBA	self-contained underwater breathing apparatus
SSSC	single sphere simple cubic

THIS PAGE INTENTIONALLY LEFT BLANK

ACKNOWLEDGMENTS

I want to thank the U.S. Navy for allowing me to study and conduct research at the Naval Postgraduate School. Thank you also to the Naval Postgraduate School and the GSEAS department. I have met the most astounding professors throughout my time here. The greatest of which is my thesis advisor, Dr. Emil Kartalov, to whom I owe a large debt of gratitude for guiding me through the rigors of research.

Also, I want to offer a special thank you to my friend and fellow student Jonathan Brown. I could not have asked for a better sounding board in both my personal and professional life. Finally, to my family, whose support throughout my life has allowed me to get to where I am now: I thank you.

THIS PAGE INTENTIONALLY LEFT BLANK

I.   INTRODUCTION

A.   BACKGROUND

"We Dive the World Over" is the motto of the U.S. Navy Diver. For decades, the U.S. Navy has conducted diving operations all over the globe. Navy Divers are critical assets for use in dive salvage, search and rescue, military missions, and more [1]. Because these divers can dive from "the darkest depths of the world's oceans to freezing arctic-like conditions underneath icebergs" [1], advanced protection is required.

1.   Dangers of Cold Water

Heat loss and core temperature are the important factors to consider when diving in cold water. While a person may be able to survive in cold weather conditions, cold water presents a larger concern. Due to the much greater thermal conductivity and specific heat of water compared to air, a diver will lose heat much faster when submerged in water than air. Figure 1 shows core body temperature of a man in bathing trunks immersed in water at 29°C [2].
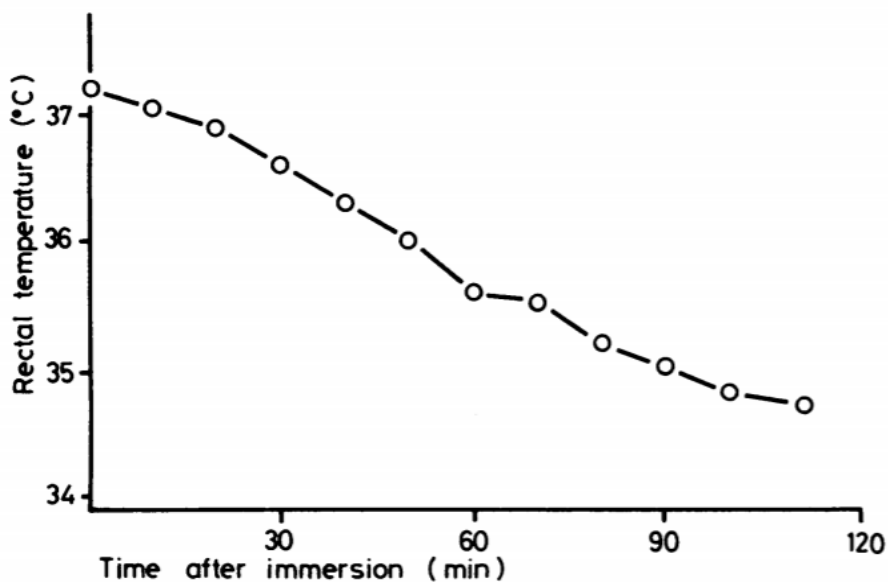
Figure 1.   Body Temperature Fall during Immersion in 29°C Water.
Source: [2].

1

It is estimated the body can only maintain thermal balance, producing as much heat as it loses, in water temperatures 95°F–96°F [3]. Once the body can no longer produce enough heat to offset the heat loss, chilling occurs. Chilling can impair dexterity and sense of touch, affecting a diver's ability to work. Chilling can also affect cognitive abilities and cause uncontrollable shivering [4].

If a diver remains in the cold environment and continues to lose heat, the next danger is hypothermia. Hypothermia is a potentially lethal condition that occurs when the core body temperature drops below 95°F or 35°C. This condition can cause further effects to the central nervous system, including loss of memory and hallucinations, and detrimental effects to the cardiovascular system. Severe cases of hypothermia can result in death if core body temperatures drop below 79°F. Hypothermia can occur even in warmer temperatures up to 91°F [4] so adequate thermal protection is important in most environments.

2.   Current Protection

The most common thermal protection divers use for temperatures above 50°F is the neoprene wet suit [4]. The wet suit works by trapping a small volume of water between the neoprene layer and the diver's skin. This water is warmed by the diver and insulated by the neoprene. For colder waters, divers may use a Variable Volume Dry Suit. Unlike the wet suit, the dry suit derives its thermal protection through additional thermal insulation worn under the suit. In a dry suit, the diver remains dry throughout the dive. Figure 2 depicts how both wet suits and dry suits insulate the diver.
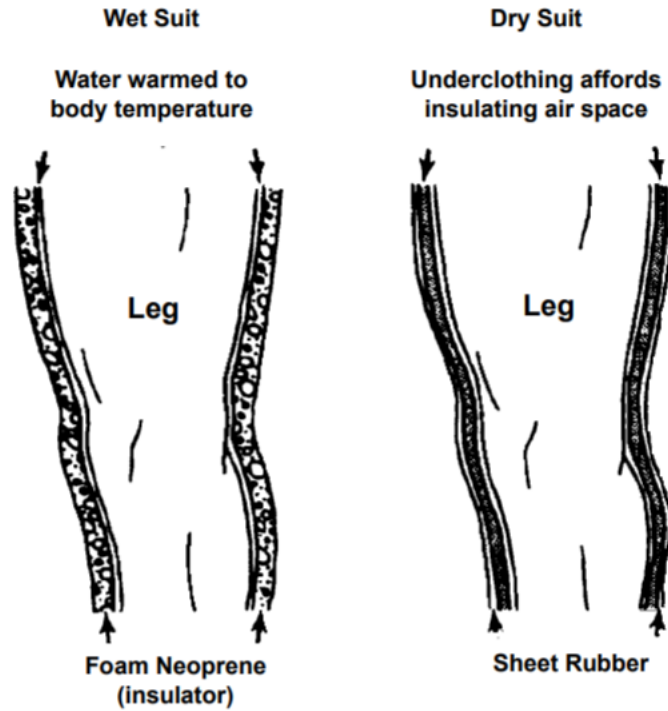
Figure 2.   Protective Clothing. Source: [5]

Neoprene, originally called DuPrene, was developed by the DuPont Company in 1930. DuPont scientists took polychloroprene, a synthetic rubber material, and used a nitrogen-based blowing agent to create a water resistant, sponge-like rubber which would later be used in wet suits [6]. This foamed neoprene can be manufactured in either an open-cell or a closed-cell configuration. Figure 3 shows a close-up of the individual cells in neoprene.
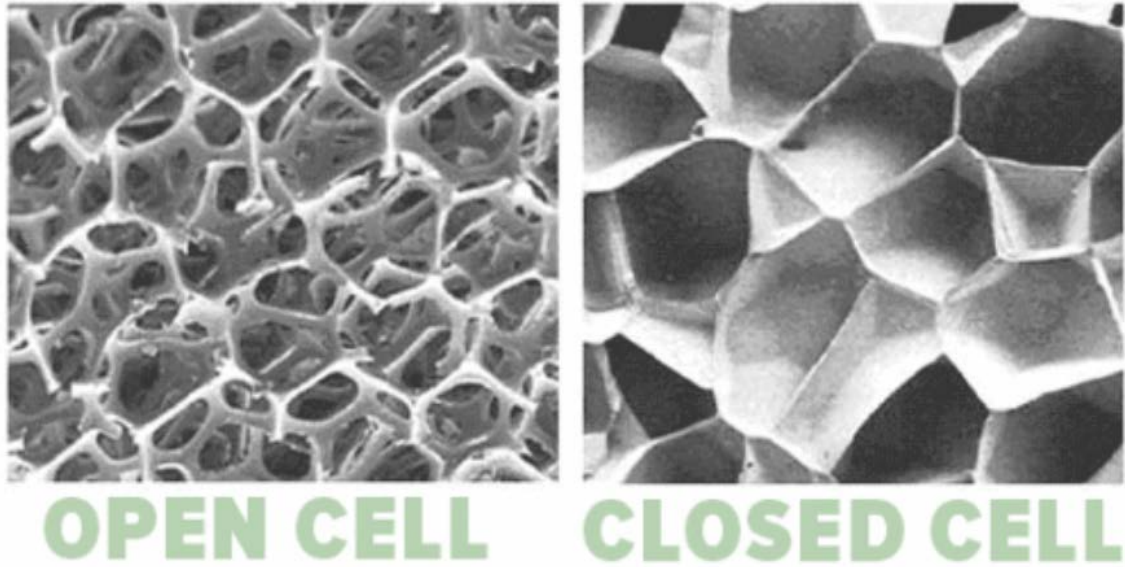
Figure 3.   Open Cell Versus Closed Cell. Source: [7].

As shown, the closed cell neoprene material is composed of small bubbles of air. Each bubble is a closed system with a fixed mass of air inside. The open cell foam allows matter, water in the case of wet suits, to pass freely through its cells. The trapped air in the closed cell foam will act as a thermal insulator and have greatly improved water resistance compared to the open cell foam [5], [7].

Dry atmospheric air is composed of approximately 78% nitrogen and 21% oxygen with several other minor gases making up the last percent [5]. The full composition of air is given in Figure 4. Once we have identified the major components of standard air, we look at the physical properties of those gases to see if there are any appreciable differences between them.

	Concentration	
Component	**Percent by Volume**	**Parts per Million (ppm)**
Nitrogen	78.084	
Oxygen	20.9476	
Carbon Dioxide	0.038	380
Argon	0.0934	
Neon		18.18
Helium		5.24
Krypton		1.14
Xenon		0.08
Hydrogen		0.5
Methane		2.0
Nitrous Oxide		0.5

Figure 4.   Components of Dry Atmospheric Air. Source: [5].

Because we are trying to increase the thermal protection of our divers' equipment, we will look at the thermal properties of the major component gases of air. The properties of concern we seek to analyze are the thermal insulating properties of our materials, specifically the thermal conductivity and specific heat seen in Table 1.

Table 1.   Comparison of Thermal Properties of Air and Common
Gases. Source: [8], [9].

	Thermal Conductivity (25°C), k $\left(\dfrac{W}{m*K}\right)$	Specific Heat, c_p $\left(\dfrac{cal}{gram*°C}\right)$
Air, dry (sea level)	0.0262	0.24
Nitrogen	0.024	0.25
Oxygen	0.024	0.22

The data shown in Table 1 indicate that the thermal properties of nitrogen are similar to standard air. We will use this similarity later in our computer modeling. These closed pockets of gas provided the thermal insulation basis for wet suit technology for almost 100 years.

B. PHYSICAL AND THERMAL PROPERTIES OF WET SUITS

1. Pressure Effects

There is a problem with closed cell construction. As the diver descends, the surrounding pressure increases due to the weight of the water overhead by approximately one atmosphere per 33 feet of seawater (FSW). Those small air pockets will experience that pressure and compress in accordance with Boyle's Law for an ideal gas [5].

$$p*V = \text{constant} \tag{1}$$

Divers may operate at various depths throughout a diving operation so it is expected the air pockets will experience various pressures during a dive. By manipulating Equation (1), we can find the following relationship:

$$p_1 V_1 = p_2 V_2$$

$$p_1 \left(\frac{4}{3} \pi r_1^3 \right) = p_2 \left(\frac{4}{3} \pi r_2^3 \right)$$

$$r_2 = r_1 \sqrt[3]{\frac{p_1}{p_2}} \tag{2}$$

Using the standard approximation in the *U.S. Navy Diving Manual* that 33 FSW is approximately one atmosphere, we can develop the graph in Figure 5.
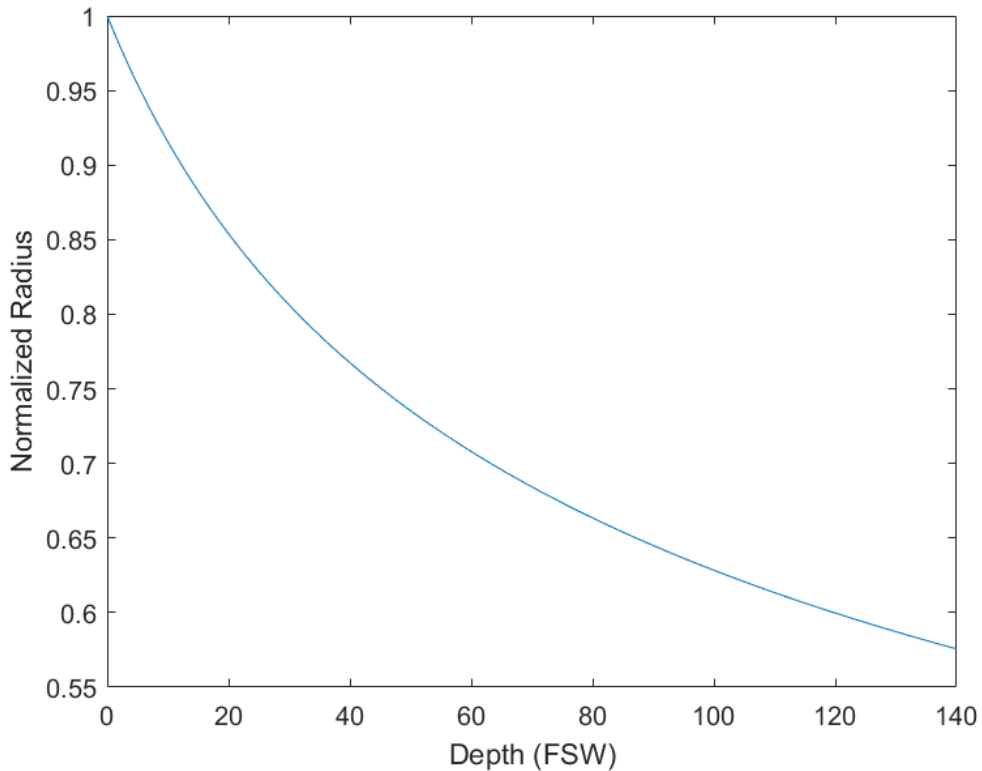
Figure 5 uses Equation (2) to plot the normalized radius of a spherical bubble of air as depth increases. This represents the change in the size of the air bubbles trapped within the neoprene material. Note that the radius, and therefore the diameter, decreases approximately 20% within the first atmosphere, which correlates to about a 48% decrease in volume.

Figure 5.   Normalized Radius of a Compressible Ideal Gas at Increasing Depth.

2.   Thermal Properties

The overall thermal conductivity of a neoprene wet suit is primarily from the air bubbles. Table 2 shows the thermal conductivities of neoprene and its components.

Table 2.   Thermal Properties of Neoprene and Its Components.
Adapted from [10], [11], [12].

	Thermal Conductivity (25°C), k $\left(\dfrac{W}{m*K}\right)$	Thermal Resistivity R $\left(\dfrac{m*K}{W}\right)$
Neoprene	0.09-0.10	10-11
Air	0.0262	38
Polychloroprene	0.19	5

Recall that neoprene is made from foamed polychloroprene. Thermal resistivity is calculated as the inverse of thermal conductivity.

As the air bubbles shrink from increasing pressure, the thermal resistivity decreases significantly as the volume of the thermally resistive air shrinks, leaving behind the more thermally conductive and less compressible polychloroprene. This reduces the volumetric percentage of air to polychloroprene and thereby reduces the overall effective thermal resistivity for the neoprene material.

Increasing pressure not only affects the volumetric percentage of air to polychloroprene, but also reduces the total thickness of the material. For this analysis, we will approximate one-dimensional heat transfer using the linear-response theory relating heat flux (φ_z) to the thermal conductivity (k) and the temperature gradient $\left(\dfrac{dT}{dz}\right)$ [13].

$$\varphi_z = -k\left(\frac{dT}{dz}\right) \tag{3}$$

Brown's experiment tested the composites by placing a disk of the material to be tested into a pressure vessel filled with ice water. A feedback-locked stage heater maintained a constant temperature of 37°C, human body temperature, on the top side of the disk. Voltage and current are measured to maintain the warm temperature. The ice water keeps the bottom of the disk at 0°C [10]. We can modify Equation (3) by substituting the heat flux with the power required to maintain the warm temperature per unit area and recalling that thermal resistivity (R) is the inverse of thermal conductivity. Also note that the temperature gradient will be opposite in direction to the heat flux. We account for this

by removing the minus sign and having $\Delta T = T_{high} - T_{low}$. Heat flux is defined as the power (W) per unit area (A). We substitute the current (I) times the voltage (V) in for power.

$$\varphi_z = \frac{W}{A} = \frac{IV}{A} = \frac{1}{R}\left(\frac{\Delta T}{L}\right) \tag{4}$$

Rearranging Equation (4) gives us the following:

$$R = \frac{A\Delta T}{(IV)L} \tag{5}$$

As the pressure increases, the radius of the air cells decreases and the neoprene material compresses, reducing the overall thickness of the material. While the material is inside the pressure vessel, it is not possible to measure thickness (L). To overcome the unknown thickness problem, Brown uses thermal insulance to compare materials under pressure. Thermal insulance (Θ) is the thermal resistivity of a material multiplied by the thickness of the material.

$$\Theta = R*L \tag{6}$$

We can substitute Equation (5) into Equation (6) to find the equation for thermal insulance.

$$\Theta = \left(\frac{A\Delta T}{(IV)\cancel{L}}\right)*\cancel{L}$$

$$\Theta = \frac{A\Delta T}{(IV)} \tag{7}$$

Equation (7) allows us to compare different materials regardless of how pressure may affect their dimensions. This analysis also assumes that electrical power is perfectly converted into thermal power. There would be small losses in energy conversion and to thermal losses to the environment, but this method allows us to effectively compare the efficacy of our materials compared to neoprene throughout the pressurization experiments. When measuring thermal properties outside of the pressure vessel thickness can be measured. With the thickness measured, resistivity can be calculated.

Overlaying the experimental data collected from Brown onto Figure 5, we notice the thermal resistivity decreases at approximately the same rate as the radius of the air cells shrink [10]. This implies a positive, direct proportionality between the size of the air cell and the insulance of the material seen in Figure 6. The decrease in insulance is predicted from Equation (6). The insulance of the neoprene decreases from the shrinking of the thermally resistive air pockets, reducing resistivity and overall thickness of the material. The disparity between the experimental data and the air cell shrinkage is expected due to other factors, such as compression of the binding elastomer, that also influence insulance. The compression of air also increases the gas's conductivity, and therefore decreases its resistivity. Higher pressure causes more molecular collisions, allowing an increased ability to transfer energy. This effect causes the neoprene material's effective resistivity to decrease even further.
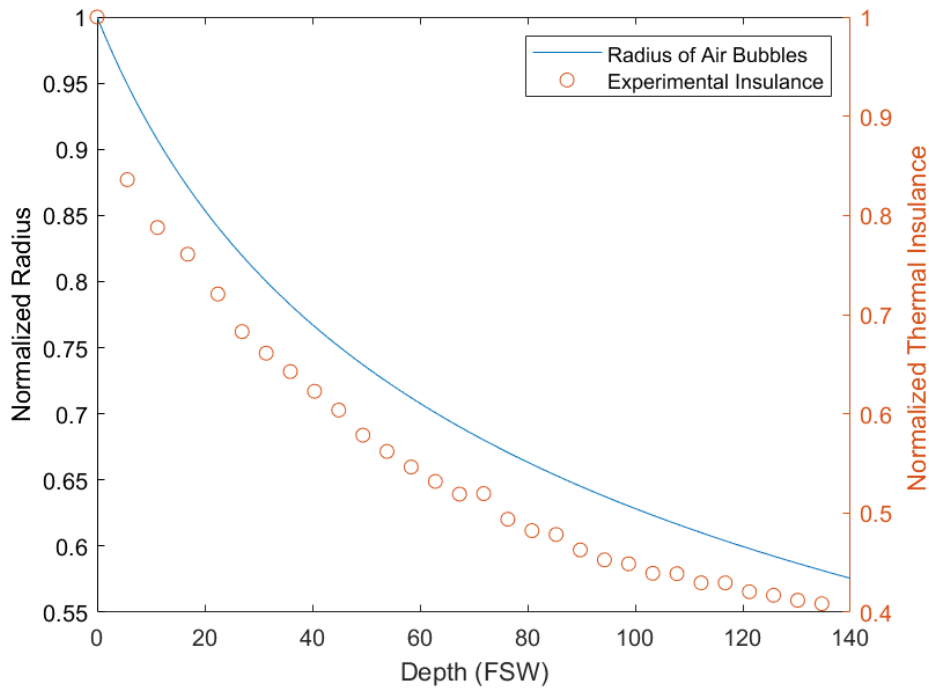
Experimental data gathered from Brown [10]. Insulance calculated using a cut out of an 8mm thick Neoprene Aqualung wet suit. The material was pressurized from 0 to 60 psig, which corresponds to depths from the surface to approximately 135 FSW.

Figure 6.   Comparison of Normalized Air Cell Radius to Normalized Thermal Insulance in Neoprene at Various Depths. Adapted from [10].

The compressibility of a wet suit's thermal insulating material is the primary factor for the reduction in thermal resistivity. For this reason, work has been done in replacing the compressible air cells with rigid, hollow glass microsphere bubbles. Figure 7 shows the results of one of Brown's pressure tests comparing the thermal insulance of neoprene and the composite material at increasing pressures.
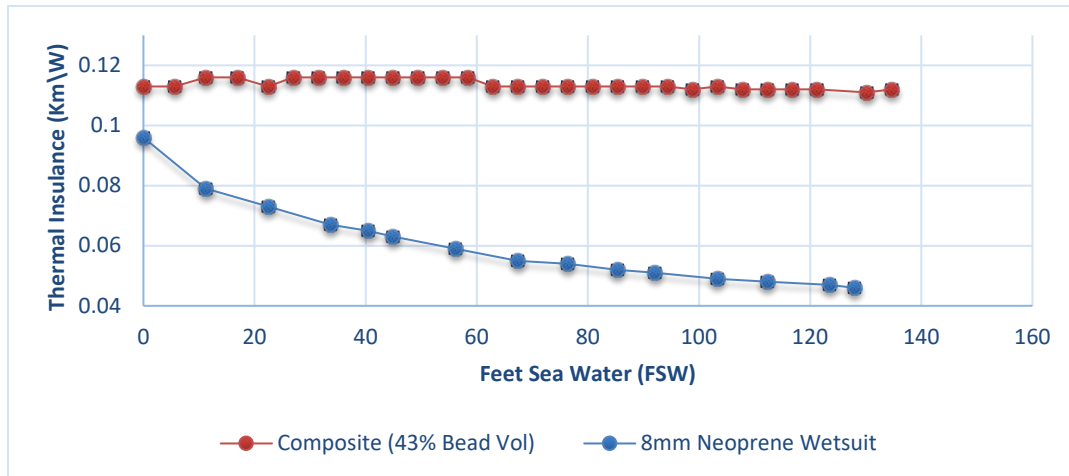
The composite material was a mixture of Sylgard 184, a polydimethylsiloxane elastomer produced by the Corning Corporation, and K1 glass microspheres from 3M.

Figure 7.   Glass Microsphere Composite Compared to a Standard Wet Suit.
Source: [10].

A cursory look at the data from Brown shows the effectiveness of the rigid microspheres compared to one of the more advanced wet suits on the market.

THIS PAGE INTENTIONALLY LEFT BLANK

II. MATERIALS AND METHODS

A. EQUIPMENT AND CONSUMABLES

In Brown's experiments, the composite materials he tested were made from rigid glass bubbles homogeneously suspended in a carrier polymer [10]. The two mixed materials were selected for their high strength and thermal properties.

1. 3M Glass Bubbles, K Series

Brown used the K1 glass bubbles [10] as the rigid spheres in his experiment. These glass bubbles are air filled soda-lime-borosilicate glass bubbles. Because the bubbles are made of glass, they are chemically stable, water resistant, non-combustible, non-porous, and non-toxic. The spherical shape allows for high strength-to-weight ratios and stable voids, leading to low and consistent thermal conductivities [14]. 3M offers many types of glass bubbles. The K1 glass bubble was selected due to its low thermal conductivity. Figure 8 shows the thermal conductivity of various glass spheres offered by 3M.

	Product	Calculated Thermal Conductivity (W·m-1·K-1) at 70°F (21°C)
K Series	K1	0.047
	K15	0.055
	K20	0.070
	K25	0.085
	K37	0.124
	K46	0.153
S Series	S15	0.055
	S22	0.076
	S32	0.108
	S35	0.117
	S38	0.127
	S38HS	0.127
	S60	0.200
	S60HS	0.200
iM Series	iM16K	0.153
	iM30K	0.200

Figure 8.   Thermal Conductivity of 3M Glass Bubbles. Source: [14].

The K1 glass bubble is also the largest of the beads, on average 65 microns [14], and the K1 glass bubble's isostatic crush strength is within acceptable levels for the pressures we expect to see while using this material in normal SCUBA diving operations [5]. Figure 9 outlines normal depths under which a Navy Diver may operate.

NORMAL AND MAXIMUM LIMITS FOR OPEN CIRCUIT SCUBA DIVING	
Depth fsw (meters)	Operational Limit
60 (18)	Maximum depth for standby SCUBA diver using a fully charged single cylinder with less than 100 SCF air available.
130 (40)	Normal working limit. Dives deeper than 130fsw may be made with approval of the Commanding Officer or Officer-in-Charge.
190 (58)	Maximum working limit.

Figure 9.   U.S. Navy Diving Restrictions for Open Circuit SCUBA Diving.
Source: [5].

The maximum rated pressure for the K1 glass bubble is 250 psi, which equates to depths exceeding 500 FSW, far beyond maximum working limits for open circuit SCUBA diving. Figure 10 shows the crush strength of other 3M glass bubbles.

	Product	Test Pressure (psi)	Target Fractional Survival	Minimum Fractional Survival
K Series	K1	250	90%	80%
	K15	300	90%	80%
	K20	500	90%	80%
	K25	750	90%	80%
	K37	3,000	90%	80%
	K46	6,000	90%	80%
S Series	S15	300	90%	80%
	S22	400	90%	80%
	S32	2,000	90%	80%
	S35	3,000	90%	80%
	S38	4,000	90%	80%
	S38HS	5,500	90%	80%
	S60	10,000	90%	80%
	S60HS	18,000	90%	90%
iM Series	iM16K	16,000	90%	90%
	iM30K	28,000	90%	90%

Figure 10. Isostatic Crush Strength for 3M Glass Bubbles. Source: [14].

While there are glass bubbles that are stronger, the K1 glass bubble is an inexpensive option with ideal thermal properties within acceptable limits.

2. Polydimethylsiloxane

The Dow Chemical Company's SYLGARD 184 silicone elastomer is the carrier polymer in Brown's experiments [10]. SYLGARD 184 is sold as a two-part, liquid component kit, which includes polydimethylsiloxane and a curing agent, which, when mixed and properly cured, will be a flexible elastomer. The expected thermal conductivity of SYLGARD 184 is $0.27 \frac{W}{m*K}$, which is close to the $0.20 \frac{W}{m*K}$ found in Brown's experiment [15], [10].

The K1 glass bubbles were homogeneously mixed into the elastomer and thoroughly degassed using an ARE-310 planetary rotary mixer made by THINKY Inc., Japan [10]. This mixture was then cured and tested for its thermal properties.

B. SOFTWARE

This thesis focuses on the simulations of the predicating theories behind Brown's experimental data. Two main programs were used. COMSOL was used to create a model

and simulate typical thermal conditions on a unit cell of the composite material developed by Brown. MATLAB was used primarily for data analytics and graphical interpretations.

1. COMSOL Multiphysics

  The COMSOL Multiphysics version 5.3 software runs a finite element analysis of multiple physical effects on computer-generated objects. Using COMSOL, one can run hundreds of different simulations quickly and economically. These simulations allow experimenters to refine their hypotheses and methods before having to expend any time or resources creating an experiment. Figure 11 shows the many different physics modules that can be used by COMSOL.

Figure 11.   Examples of Physics Modules COMSOL Can Use. Source: [16].

The multiphysics modules allow users to combine properties from several different areas of study. Combining many modules could allow a user to study time dependent or stationary effects of how thermal dissipation from an AC power source would deform

materials attached to the system. COMSOL's ability to import CAD models can allow engineers to quickly determine any flaws in their systems before they even build it [16].

COMSOL has been used as a method of solving simple to complex heat transfer problems. In Xiong's paper, he solves three fairly simple problems concerning heat loss from one side of a wall to another [17]. This is a trivial problem even to solve by hand but demonstrates how COMSOL can be used to solve thermal problems. Berne used COMSOL to validate, or in the case of his paper, raise questions, findings on nanoparticles suspended in a fluid [18], shown in Figure 12. His paper provided the basis of how we developed our own experimental model in COMSOL.
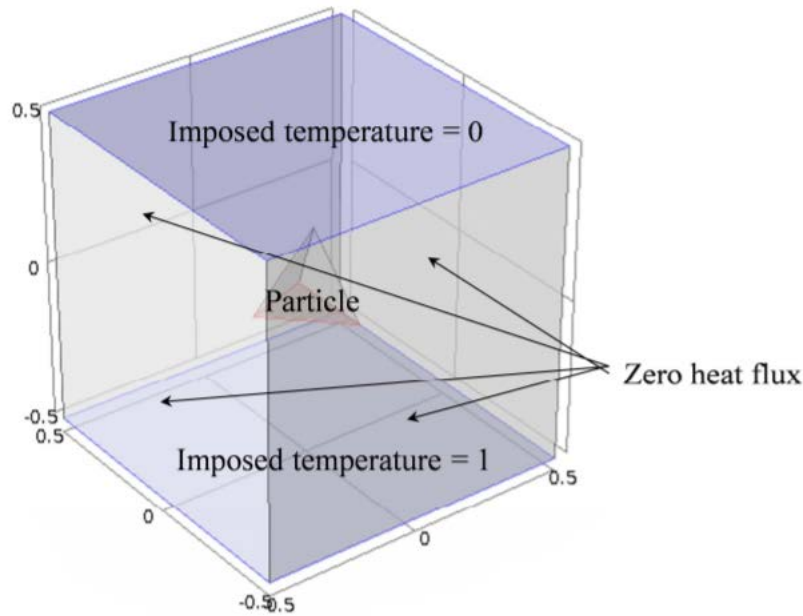
Figure 12.　Domain and Boundary Conditions from Berne. Source: [18].

For our glass bubble experimentation, we set up a similar model using our K1 glass bubble as the particle and varying the size instead of the shape and orientation. We used the Heat Transfer in Solids physics module for our simulation. While other physics modules could have been used, such as thermal stress or thermoelasticity from the Structural Mechanics modules, the difference between the inclusions of additional physics

18

modules to the parameters we are measuring would be minor compared to the increased computational load required to run the more complex model. Of course, there will be stresses caused by the change from body temperature to freezing in the composite material, but the effects on net heat flux and thermal resistivity would be negligibly small and we do not anticipate any adverse effects to the structural integrity of the glass spheres large enough to cause breakage. Therefore, to simplify our simulation without losing information, we only selected the one physics module, Heat Transfer in Solids.

2. MATLAB R2018a

MATLAB was primarily used as a data analysis tool and graphing tool. Data was pulled from COMSOL into MATLAB where it could be more easily processed.

THIS PAGE INTENTIONALLY LEFT BLANK

III.   DESIGN CHARACTERISTICS

A.   THE UNIT CELL

K1 microspheres range from about 30 microns to a maximum size of 120 microns. To perfectly model our material in COMSOL, we would have to program a simulation creating millions of tiny bubbles of random sizes and orientations in a PDMS disk. While possible, the computing power required to solve this problem is so large that it is infeasible to develop a model this way.

Thermal resistivity is an intrinsic material property independent of mass or size. Because resistivity is intrinsic, we can use a unit cell for our model. Berne used a similar concept to model nanoparticles suspended in a fluid [18]. In our models, we designed a unit cell with different cubic structures to mimic a finite piece of our materials. To represent changes in volumetric densities of glass bubbles to the carrier polymer, we varied the radius of the internal spherical segments to increase or decrease the volumetric ratio of spheres to the cube.

$$\text{Volumetric Percentage} = \frac{\text{Volume of Spheres}}{\text{Volume of Cube}} \times 100 \qquad (8)$$

We also calculate the largest radius that the spherical objects can have and still be within the boundaries of the cube. The maximum radius will set the maximum size and volume of the spheres. Understanding the geometric limitations of the model is important for COMSOL because the program will continue to calculate values even when the sphere objects are outside the boundaries or overlapping one another. This will cause COMSOL to output incorrect and misleading data.

1.   Single Sphere Simple Cubic (SSSC)

Our model uses a modification of the simple cubic structure. Rather than using a cube with $\frac{1}{8}$ a sphere in each corner, we placed one intact sphere in the center of the cube. When propagated, this unit cell will have the same properties in both models. Figure 13 is the model used for the SSSC.
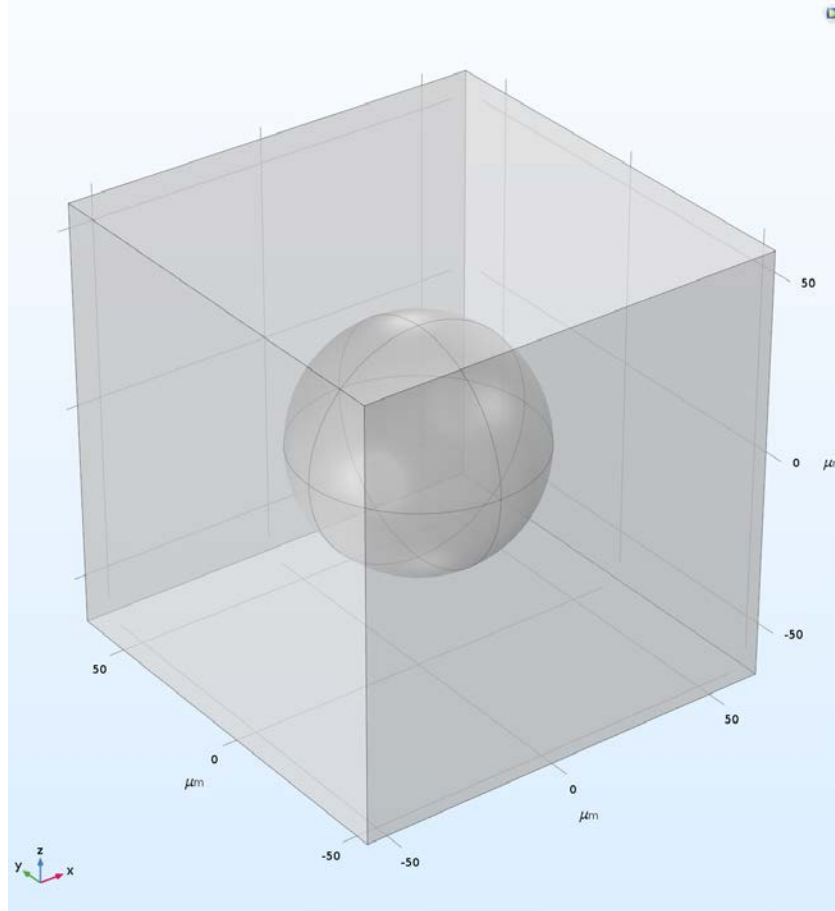
Model created in COMSOL.

Figure 13. Single Sphere Simple Cubic.

To calculate the volumetric percentage, we use Equation (8).

$$\text{Volumetric Percentage} = \frac{\text{Volume of Spheres}}{\text{Volume of Cube}} \times 100$$

$$\text{Volumetric Percentage}_{\text{Simple Cubic}} = \frac{\frac{4}{3}\pi r^3}{a^3} \times 100 \tag{9}$$

The maximum radius for the single sphere simple cubic is when the center sphere is fully transcribed within the cube. This occurs when the radius is half the value of the cube's side length. Using Equation (9), we see that the maximum percentage is approximately 52.4%.

$$\text{Volumetric Percentage}_{\text{Simple Cubic}} = \frac{\frac{4}{3}\pi\left(\frac{a}{2}\right)^3}{a^3} \times 100$$

$$= \frac{\frac{4}{3}\pi\frac{a^3}{8}}{a^3} \times 100 \approx 52.4\%$$

The rated packing factor of the K1 glass bubbles "averages about 60%" [14]. This is largely due to the inhomogeneity of the glass bubble sizes. Smaller bubbles are able to fill in the voids the larger bubbles create. While the SSSC may not perfectly reflect the composite material, it is a simple design and can be used to approximate the behavior of the material.

2. Body-Centered Cubic (BCC)

The BCC model is the model we suspect the glass bubbles resemble the most. This configuration fits two whole sphere volumes within the cube. Figure 14 is the model used for the BCC.
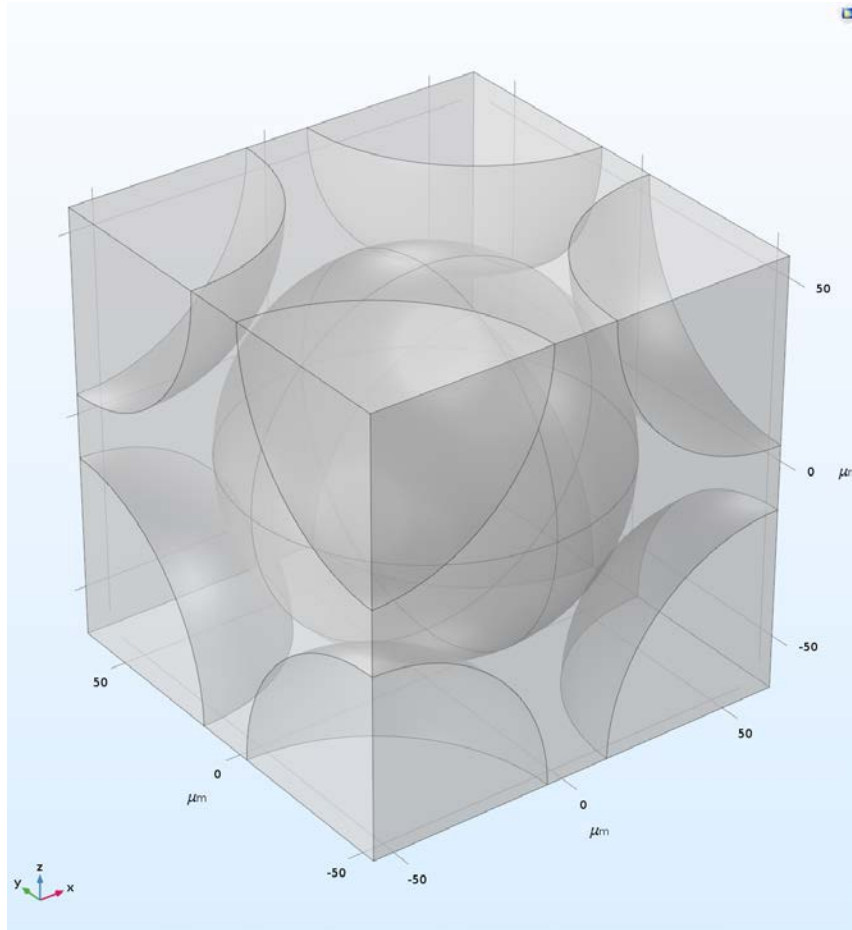
Model created in COMSOL.

Figure 14.   Body Centered Cubic.

This slightly changes our volumetric percentage equation:

$$\text{Volumetric Percentage}_{\text{BCC}} = \frac{2 \times \left(\frac{4}{3}\pi r^3\right)}{a^3} \times 100 \qquad (10)$$

Looking at the BCC model, the main diagonal of the cube is four times the radius when the spheres are at their largest. Using this identity, the relationship between the side length and the radius is:

$$r_{\max} = a\sqrt{\frac{3}{16}}$$

24

We can substitute the maximum radius into Equation (10) to find the maximum volumetric percentage in the BCC configuration.

$$\text{Volumetric Percentage}_{\text{BCC}} = \frac{2 \times \left(\frac{4}{3}\pi r^3\right)}{a^3} \times 100$$

$$= \frac{2 \times \left(\frac{4}{3}\pi \left(a\sqrt{\frac{3}{16}}\right)^3\right)}{a^3} \times 100$$

$$= \frac{\frac{8}{3}\pi a^3 \left(\sqrt{\frac{3}{16}}\right)^3}{a^3} \times 100 \approx 68.0\%$$

This packing factor is higher than the stated packing factor of the K1 beads.

3.   Face-Centered Cubic

The face-centered cubic (FCC) is the most efficient method to pack equal-size spheres into a cubic volume. Figure 15 is the model used for the FCC.
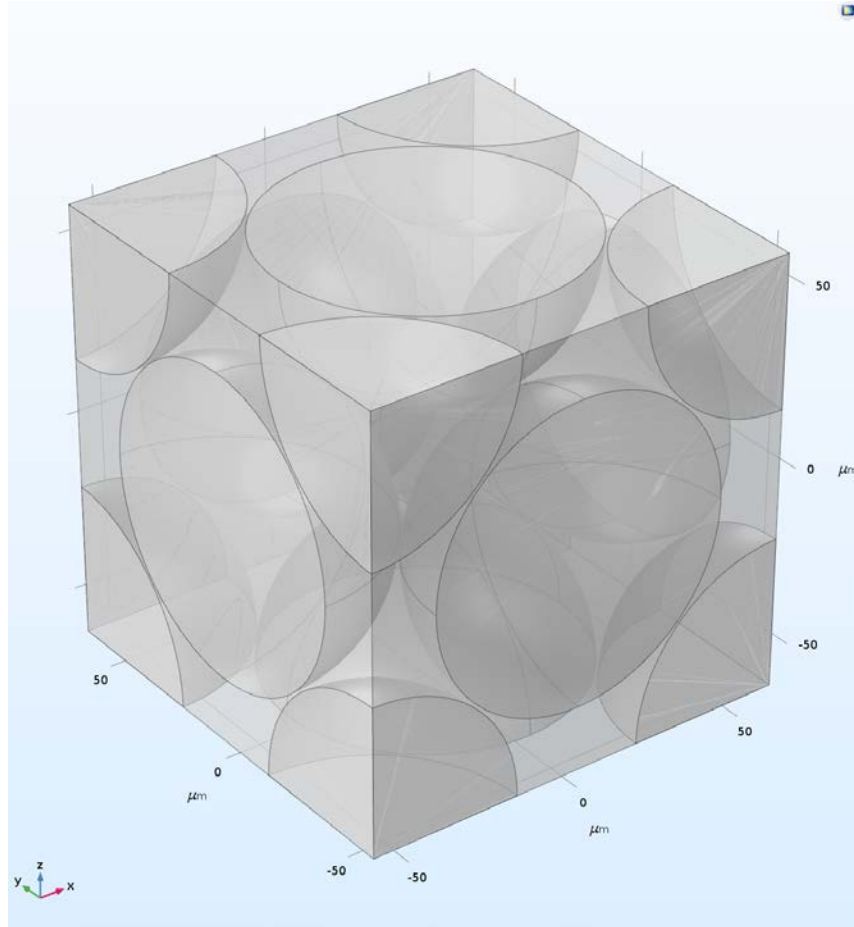
Model created in COMSOL

Figure 15.   Face Centered Cubic

This configuration can fit four spherical volumes within the unit cell, giving a much higher packing factor:

$$\text{Volumetric Percentage}_{\text{FCC}} = \frac{4 \times \left(\frac{4}{3} \pi r^3 \right)}{a^3} \times 100 \qquad (11)$$

The maximum radius of the spheres is a quarter of the diagonal along the faces of the cube. Calculating the relationship yields the following maximum radius:

$$r_{\max} = a \sqrt{\frac{1}{8}}$$

Substituting the maximum radius into Equation (11) gives us a much higher packing factor than the other configurations:

$$\text{Volumetric Percentage}_{FCC} = \frac{4 \times \left(\frac{4}{3} \pi \left(a \frac{1}{\sqrt{8}} \right)^3 \right)}{a^3} \times 100$$

$$= \frac{\frac{16}{3} \pi a^3 \left(\frac{1}{\sqrt{8}} \right)^3}{a^3} \times 100 \approx 74.0\%$$

This is well beyond the factory stated packing factor of the K1 glass bubbles of about 60% [14]. We will still develop a model for the FCC structure for use as an upper bound. The composite material is a mixture of many sized K1 glass bubbles and the 60% packing factor is only an average. A cubic structure with a denser packing factor should be able to account for small discrepancies stemming from small glass bubbles filling any voids created by larger glass bubbles.

B.   SPHERICAL MATERIAL MODELS

Per the 3M technical specifications, the K1 glass bubbles have an average effective thermal conductivity of $0.047 \left(\frac{W}{m*K} \right)$ [14]. While this value works for a macro analytical value, we will analyze our unit cell at the micro level. For this, we must take into account any shunting effects the material composition of the beads may cause. The glass bubbles themselves are tiny air pockets encapsulated in a soda-lime-borosilicate glass [14]. Each of the materials we are analyzing have large differences in thermal conductivity outlined in Table 3.

Table 3.   Thermal Properties of Composite Materials. Adapted from
[9], [10], [14], [19].

	Thermal Conductivity (25°C), k $\left(\dfrac{W}{m*K} \right)$	Thermal Resistivity R $\left(\dfrac{m*K}{W} \right)$
K1 Technical Data Sheet	0.047	21
Air	0.0262	38
Glass	1 - 1.30	0.8 - 1
PDMS	0.20	5

Thermal resistivity is calculated as the inverse of thermal conductivity.

Table 3 shows that the K1 glass bubble rated thermal conductivity is some average between the outer glass shell and the air on the inside. Because of the variation in conductivities of the composite materials, we will model the glass bubbles in three ways.

1.   Air Spheres

The first model will model the K1 glass spheres as air. The majority of the volume of the glass bubbles is air. The glass is only a thin shell encapsulating the air. Using COMSOL, we will assign the thermal properties of the spheres as the standard air in the program.

2.   Technical Data

The second simulation will replace the thermal conductivity of air with the expected thermal conductivity for the K1 glass bubbles given to us by the 3M's technical data sheet.

3.   Glass-Air Bubble

The final simulation will be the most computationally demanding. We model the actual glass bubble, creating a thin glass shell with a large air volume encased within it. One factor that had to be calculated was the thickness of the glass shell. This was done by taking the expected densities of the K1 glass spheres, soda-lime-borosilicate glass, and air

and solving for the percent volume ratios of air to glass. From this, we were able to calculate the thickness of the highly thermally conductive glass shell, drawn in Figure 16.

There is no technical data regarding the specifics of shell thickness. To determine the thickness of the glass bubble, we calculate the ratio of densities and volumes for a typical glass bubble. Figure 16 shows a hypothetical cross-section of the glass bubble.
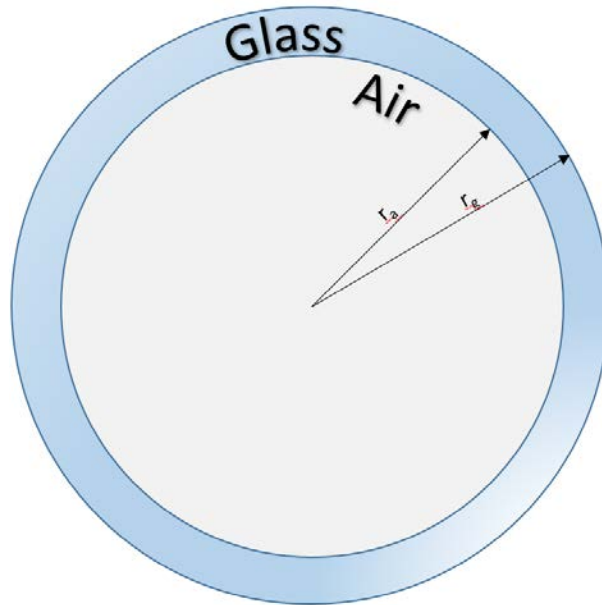
Figure 16.   Drawing of the K1 Glass Bubble.

Starting with the conservation of mass, the mass of the bead, m_b, is the sum of the mass of the air and glass, m_a and m_g, respectively.

$$m_b = m_a + m_g \tag{12}$$

Substituting the density equation into Equation (12) yields:

$$\rho = \frac{m}{V}$$
$$m = \rho * V$$

$$\rho_b V_b = \rho_a V_a + \rho_g V_g \tag{13}$$

29

Ultimately, we are looking for the ratio between the radii of the interior and exterior of the glass bubble.

$$\rho_b(\frac{4}{3}\pi r_b^3) = \rho_a(\frac{4}{3}\pi r_a^3) + \rho_g[\frac{4}{3}\pi(r_g^3 - r_a^3)] \tag{14}$$

The radius of the glass bubble, r_b, is equivalent to the radius of the glass, r_g. Note that the volume of the glass requires removing the volume of the internal air bubble; those adjustments are seen in Equation (14). Cleaning up some of the variables and like terms allows us to find the ratio of radii.

$$\rho_b r_g^3 = \rho_a r_a^3 + \rho_g r_g^3 - \rho_g r_a^3$$

$$\rho_b = \rho_a \frac{r_a^3}{r_g^3} + \rho_g - \rho_g \frac{r_a^3}{r_g^3}$$

$$\rho_b - \rho_g = \frac{r_a^3}{r_g^3}(\rho_a - \rho_g)$$

$$\frac{r_a^3}{r_g^3} = \frac{\rho_b - \rho_g}{\rho_a - \rho_g}$$

$$\frac{r_a}{r_g} = \sqrt[3]{\frac{\rho_b - \rho_g}{\rho_a - \rho_g}} \tag{15}$$

From here, we used the following typical densities:

Table 4.   Table of Densities. Adapted from [14], [19], [20].

	Density $\left(g/cm^3 \right)$
K1 Glass Bubble	0.125
Borosilicate Glass	2.20
Air (at 25°C)	1.18 x 10^{-3}

The ratio of the air to glass radii is approximately 98.1%. This high ratio is expected because the glass shell is very thin.

C. THERMAL CONDITIONS

To mimic Brown's experimental data, we set the top plane of our unit cube to 310 °K, approximately human body temperature, and the bottom plane to 273.15 °K, the freezing temperature of water. Initial conditions for the cube was set to 310 °K. The initial temperature was chosen under the assumption a diver's suit would be approximately body temperature when sitting on the surface. Because we are doing a stationary, time independent analysis, the initial temperature does not matter for the COMSOL calculations of resistivity and conductivity, as these are temperature independent properties so long as the temperature does not change significantly. However, to correctly calculate heat flux and to maintain the similarity of the model to the experiment, we still used body temperature as the initial temperature.

Thermal insulation set the heat flux from the side walls to zero. Brown's experiment was designed to cause mono-directional heat flow through the composite disk [10]. To simulate this, we will remove any edge effects by prohibiting heat flow out of the side faces of our cube.

D. STUDY PARAMETERS

1. Mesh Considerations

COMSOL primarily uses Finite Element Modeling (FEM) as its analysis technique [16]. As such, COMSOL will develop a three dimensional mesh composed of small, three-dimensional elements. The smaller the volume of each element, the better granularity the solution will have. The cost of a smaller element mesh is computational power. Our analysis involved analyzing shunting effects of different elements with different thermal conductivities. To ensure the greatest accuracy, the predefined 'Extra fine' physics controlled mesh was primarily used throughout the experiment. Due to the relatively simplistic geometries of our model, the small element size was not prohibitively

computationally intensive. Finer element sizes on the SSSC were tested with negligible differences in accuracy.

2.   Stationary Parametric Sweep

As mentioned, a stationary analysis was used. Thermal resistivity is not time dependent, so a steady state analysis was chosen. The Parametric Sweep option was used. This option allows us to sweep a particular parameter across a range of values and study the effects. In our analysis, we swept the radius of the spheres from 1 µm to a value close but not exceeding the maximum radius that can fit into a unit cell for a particular configuration. Recall from the previous equations, the maximum radius for the SSSC, BCC, and FCC configurations were approximately 50%, 43%, and 35% of the length of the cube, respectively.

IV. RESULTS AND ANALYSIS

A. RESULT ANALYSIS

Once all the initial conditions and parameters were set, the simulation was run for each geometric configuration and material. For each experiment, the volumetric percentage and resistivity were calculated. The volumetric percentage equations from before were used:

$$\text{Volumetric Percentage}_{SSSC} = \frac{\frac{4}{3}\pi r^3}{a^3} \times 100$$

$$\text{Volumetric Percentage}_{BCC} = \frac{2 \times \left(\frac{4}{3}\pi r^3\right)}{a^3} \times 100$$

$$\text{Volumetric Percentage}_{FCC} = \frac{4 \times \left(\frac{4}{3}\pi r^3\right)}{a^3} \times 100$$

To calculate resistivity we use a modified version of Equation (5) where we substitute heat flux back in for the current and voltage and take in account that the area of a cube face is L^2:

$$R = \frac{A\Delta T}{(IV)L}$$

$$R = \frac{L\Delta T}{\varphi_z} \tag{16}$$

The heat flux (φ_z) used is the total net heat rate passing through the freezing plane. COMSOL recognizes this variable as *ht.temp2.ntfluxInt*. The side-length of the cube is simply defined as the variable *length*. The difference in temperature is the difference between the top heated plane and bottom freezing plane. Inserting the constants and the variable into Equation (17) we get the full equation for resistivity used by COMSOL:

$$R = \frac{length * (310 - 273.15)}{ht.temp2.ntfluxInt} \tag{17}$$

B. MATERIAL EFFECTS

Figure 17 provided us with very promising data. As expected, pure air spheres were the most thermally resistive composite material and the glass shell spheres were the lowest. These two materials encompass the majority of the data points. The spheres set to the 3M issued thermal rating were in between the air and glass shelled spheres, where most of the experimental data were observed to be.
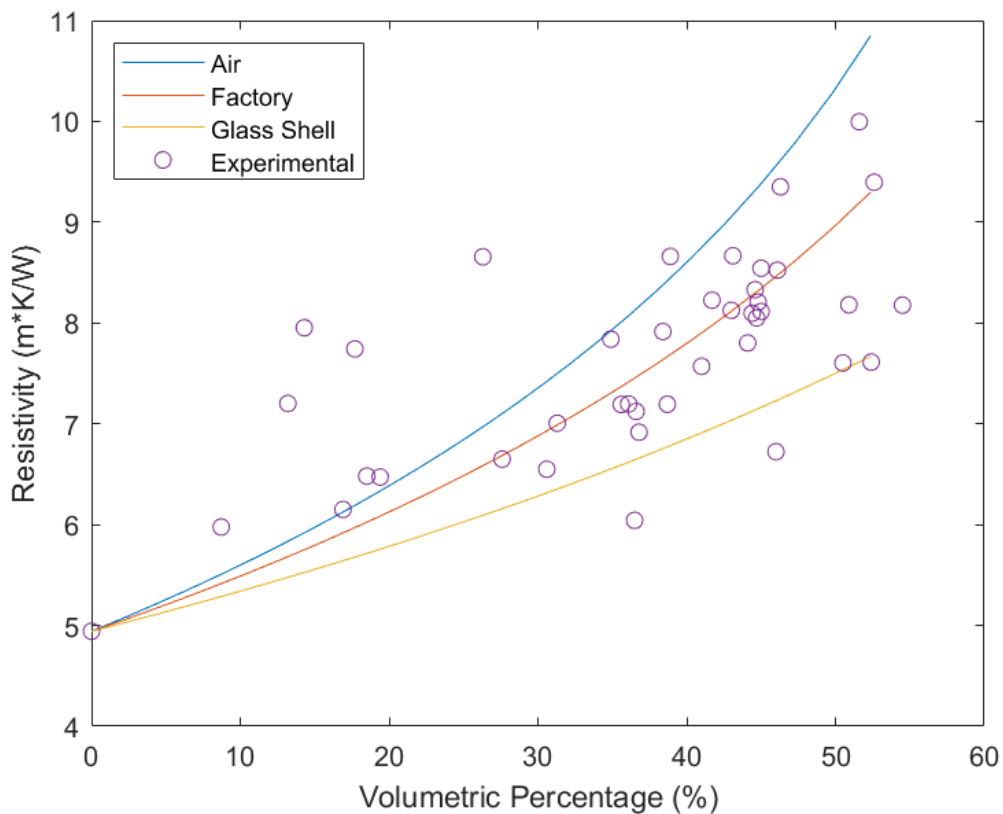
Experimental data from Brown, analysis conducted with COMSOL using the SSSC configuration.

Figure 17.   Comparison of Different Sphere Materials to Experimental Data. Adapted from Brown [10].

This analysis shows that the thermal conductivity given by 3M is fairly accurate and is sufficient to use in predicting the characteristics of the composite material.

C.   STERIC CONFIGURATION

Figure 18 shows the differences in the steric configurations using the 3M thermal rating. As shown, there are very minor differences. The same is true for the air spheres and glass shell spheres. Recall that the maximum packing factor is different for each configuration, which is reflected in the graph.
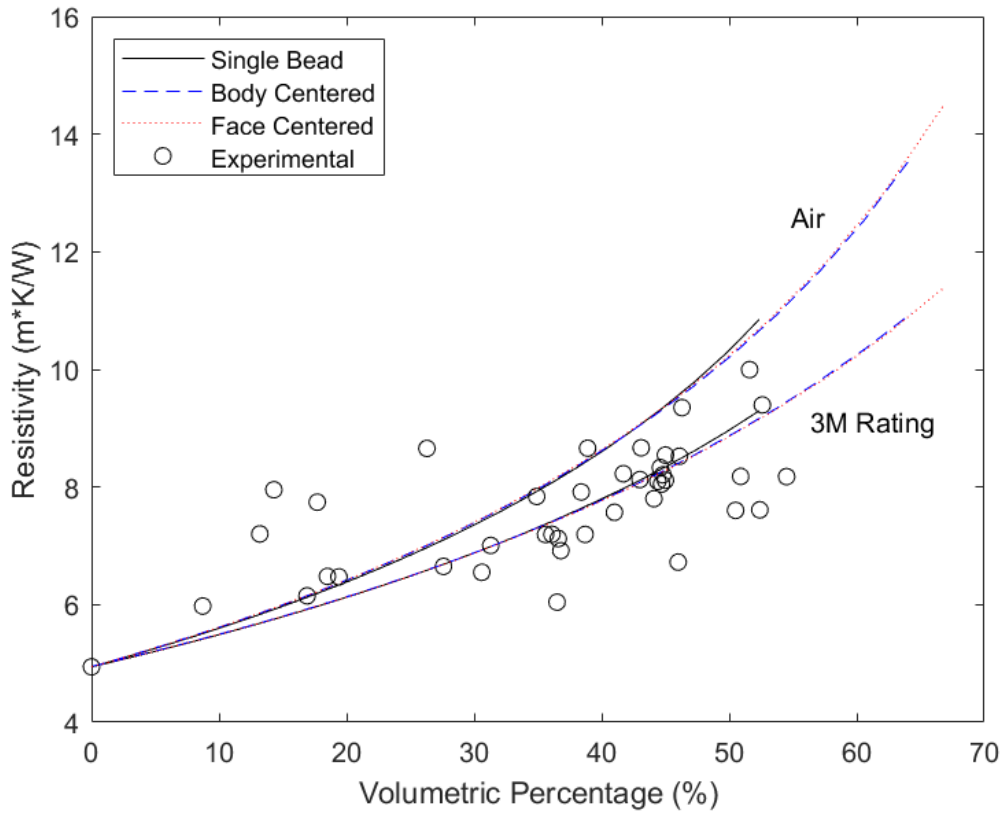
Figure 18.   Comparison of Different Steric Configurations
with 3M Thermal Ratings

The computational power required for a complete analysis of all configurations of the glass shells would be too great. The glass shell is very thin compared to the total volume of the sphere and to get a proper analysis at smaller volumetric percentages would require more computing power than currently available at the laboratory. It is expected that the different glass sphere configurations will not be a major factor in resistivity calculations

and will likely follow the resistivity of the SSSC configuration. Because of this, a complete parametric analysis was not done for the glass sphere material for the BCC and FCC configurations.

V. BREAKAGE ANALYSIS

A. EXPECTED BREAKAGE

While the K1 glass bubbles are strong enough to withstand pressures at typical operating depths, there is a small fraction of bubbles that are expected to be destroyed during the manufacturing process. We took steps to minimize this fraction by using a planetary mixer. This type of mixer combines the glass bubbles with the carrier polymer by rotating the mixture at high speeds on multiple axes instead of using a rod to stir the composite, which could potentially break the glass shells.

Breakage causes the release of thermally resistive air in our composite, leaving behind the highly conductive glass shell, which lowers the overall resistivity of the composite. Due to the degassing process during manufacturing of the composite, the released air should be removed and not impact our experiment. Using the densities and resistivities of the composite material and its individual components, we developed a method of predicting the percentage of breakage within the system.

1. Alpha and Beta

We will first define Alpha as the fractional volume of the intact glass bubbles and Beta as the fractional volume of the glass left behind by broken glass bubbles.

$$\alpha \equiv \frac{V_B}{V_T} \tag{18}$$

$$\beta \equiv \frac{V_G}{V_T} \tag{19}$$

Next, we will assume that the volume of the composite is the sum of the volumes of its components.

$$V_T = V_P + V_G + V_B$$

From this relationship, we can solve for the fractional volume of the carrier polymer.

$$V_p = V_t - V_g - V_b$$
$$V_p = V_t - V_t\beta - V_t\alpha$$

$$\frac{V_p}{V_t} = (1 - \beta - \alpha) \tag{20}$$

Now, we use the conservation of mass principles to solve for Alpha in terms of the densities of the materials and Beta:

$$\rho_t = \frac{\sum m_i}{\sum V_i}$$

$$\rho_t = \frac{m_g + m_b + m_p}{V_g + V_b + V_p}$$

$$\rho_t = \frac{\rho_g V_g + \rho_b V_b + \rho_p V_p}{V_g + V_b + V_p}$$

$$\rho_t (V_g + V_b + V_p) = \rho_g V_g + \rho_b V_b + \rho_p V_p$$

$$\rho_t V_g + \rho_t V_b + \rho_t V_p = \rho_g V_g + \rho_b V_b + \rho_p V_p$$

$$(\rho_t - \rho_g)V_g + (\rho_t - \rho_b)V_b + (\rho_t - \rho_p)V_p = 0$$

At this point, we will substitute in our Alpha and Beta terms:

$$(\rho_t - \rho_g)\cancel{V_t}\beta + (\rho_t - \rho_b)\cancel{V_t}\alpha + (\rho_t - \rho_p)\cancel{V_t}(1 - \beta - \alpha) = 0$$

$$(\rho_t - \rho_g)\beta + (\rho_t - \rho_b)\alpha + (\rho_t - \rho_p)(1 - \beta - \alpha) = 0$$

$$\cancel{\rho_t\beta} - \rho_g\beta + \cancel{\rho_t\alpha} - \rho_b\alpha + \rho_t - \rho_p \cancel{- \rho_t\beta} + \rho_p\beta \cancel{- \rho_t\alpha} + \rho_p\alpha = 0$$

$$(\rho_p - \rho_b)\alpha + (\rho_p - \rho_g)\beta + \rho_t - \rho_p = 0$$

$$(\rho_p - \rho_b)\alpha = \rho_p - \rho_t - (\rho_p - \rho_g)\beta$$

Finally, solving for Alpha, we get our first equation:

$$\alpha = \frac{\rho_p - \rho_t - (\rho_p - \rho_g)\beta}{(\rho_p - \rho_b)} \tag{21}$$

Next, we need another equation for Alpha. We modeled our material similarly to parallel resistors. We used three equal length thermal pathways with varying radii to represent our material. The differences in radii will account for the differences in volume each component contributes to the composite. Assuming the parallel configuration more

closely models the shunting effect we predict occurs from the individual components of the composite, each with a different resistivity. To find total thermal conductance from components in parallel, one only has to add the individual conductance for each material [13]. Because our experiments deal with resistivity, we must add the inverse thermal resistances (T) to each other.

$$\frac{1}{T_t} = \frac{1}{T_b} + \frac{1}{T_g} + \frac{1}{T_p}$$ (22)

Where the thermal resistance is equal to the resistivity (R) multiplied by the length, divided by the cross-sectional area.

$$T = \frac{RL}{A}$$ (23)

In many textbooks, the resistivity is often represented by rho and the thermal resistance is represented by R. Since we will be using densities in our calculations, we define rho as a density and R as a resistivity. Substituting Equation (23) into Equation (22) yields:

$$\frac{A_t}{R_t L} = \frac{A_b}{R_b L} + \frac{A_g}{R_g L} + \frac{A_p}{R_p L}$$

In our configuration, all the lengths are the same so they will divide out, but the cross-sectional areas will differ. We will also multiply the entire equation by L to get volume terms in the numerators. This gives us the following equation:

$$\frac{V_t}{R_t} = \frac{V_b}{R_b} + \frac{V_g}{R_g} + \frac{V_p}{R_p}$$ (24)

Substituting our fractional volume terms into Equation (24) will give us our second Alpha equation.

$$\frac{V_t}{R_t} = \frac{\alpha V_t}{R_b} + \frac{\beta V_t}{R_g} + \frac{(1-\beta-\alpha)V_t}{R_p}$$

$$\frac{1}{R_t} = \frac{\alpha}{R_b} + \frac{\beta}{R_g} + \frac{(1-\beta)}{R_p} - \frac{\alpha}{R_p}$$

$$\alpha(\frac{1}{R_b} - \frac{1}{R_p}) = \frac{1}{R_t} - \frac{\beta}{R_g} - \frac{1-\beta}{R_p}$$

$$\alpha = \frac{\dfrac{1}{R_t} - \dfrac{1}{R_p} + \beta(\dfrac{1}{R_p} - \dfrac{1}{R_g})}{\dfrac{1}{R_b} - \dfrac{1}{R_p}} \tag{25}$$

Setting Equation (21) and Equation (25) equal to each other yields:

$$\frac{\rho_p - \rho_t - (\rho_p - \rho_g)\beta}{(\rho_p - \rho_b)} = \frac{\dfrac{1}{R_t} - \dfrac{1}{R_p} + \beta\left(\dfrac{1}{R_p} - \dfrac{1}{R_g}\right)}{\dfrac{1}{R_b} - \dfrac{1}{R_p}}$$

$$\left(\frac{1}{R_b} - \frac{1}{R_p}\right)\left(\rho_p - \rho_t - (\rho_p - \rho_g)\beta\right) = (\rho_p - \rho_b)\left[\frac{1}{R_t} - \frac{1}{R_p} + \beta\left(\frac{1}{R_p} - \frac{1}{R_g}\right)\right]$$

$$\frac{\rho_p}{R_b} - \frac{\rho_t}{R_b} - \frac{\rho_p\beta}{R_b} + \frac{\rho_g\beta}{R_b} - \frac{\rho_p}{R_p} + \frac{\rho_t}{R_p} + \frac{\rho_p\beta}{R_p} - \frac{\rho_g\beta}{R_p} = \frac{\rho_p}{R_t} - \frac{\rho_p}{R_p} + \frac{\rho_p\beta}{R_p} - \frac{\rho_p\beta}{R_g} - \frac{\rho_b}{R_t} + \frac{\rho_b}{R_p} - \frac{\rho_b\beta}{R_p} + \frac{\rho_b\beta}{R_g}$$

$$\beta\left(\frac{\rho_p}{R_g} - \frac{\rho_b}{R_g} + \frac{\rho_b}{R_p} - \frac{\rho_g}{R_p} + \frac{\rho_g}{R_b} - \frac{\rho_p}{R_b}\right) = \left(\frac{\rho_p}{R_t} - \frac{\rho_b}{R_t} + \frac{\rho_b}{R_p} - \frac{\rho_t}{R_p} + \frac{\rho_t}{R_b} - \frac{\rho_p}{R_b}\right)$$

$$\beta = \frac{\left(\dfrac{\rho_p - \rho_b}{R_t} + \dfrac{\rho_b - \rho_t}{R_p} + \dfrac{\rho_t - \rho_p}{R_b}\right)}{\left(\dfrac{\rho_p - \rho_b}{R_g} + \dfrac{\rho_b - \rho_g}{R_p} + \dfrac{\rho_g - \rho_p}{R_b}\right)} \tag{26}$$

Now that we have equations for Alpha and Beta in terms of known resistivities and densities, we can estimate the breakage values from Brown's experiments.

2. Analysis

With our Alpha and Beta terms, we can use the experimental data from Brown's work to look at the effects of breakage. First, we will look at Alpha. Recall that Alpha was

the volumetric ratio of intact glass bubbles to the total volume. Brown calculated an estimated bead percentage using a ratio of densities between the composite, polymer, and intact glass bubbles.

$$\text{Bead Percentage} = \frac{\rho_p - \rho_t}{\rho_p - \rho_b}$$

Comparing Brown's calculated bead percentage to ours results in Figure 19.
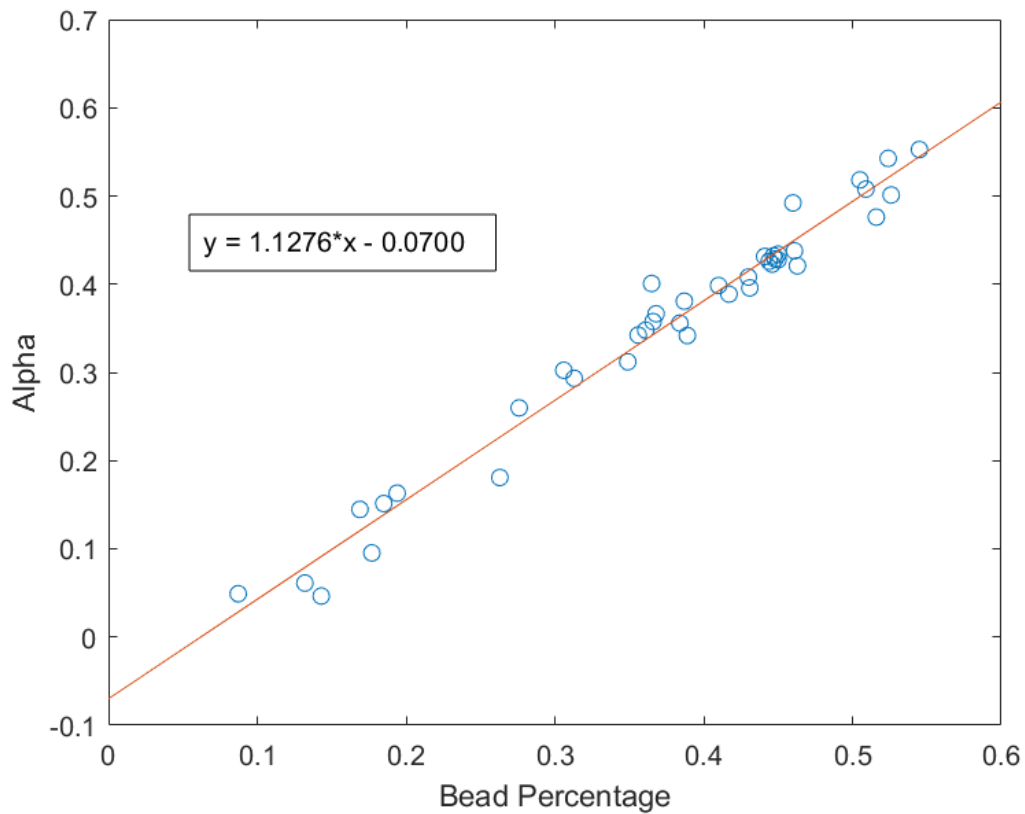
Figure 19. Alpha Compared to Experimental Bead Percentage.
Adapted from [10].

There is a strong positive correlation between Alpha and the bead percentage. This is unsurprising since Alpha is defined similarly to how Brown defined Bead Percentage. Looking into the equations done by Brown [10] (subscripts changed for continuity) and comparing them to our Alpha shows the difference:

41

$$\text{Bead Percentage} = \frac{\rho_p - \rho_t}{\rho_p - \rho_b} \qquad \alpha = \frac{\rho_p - \rho_t - (\rho_p - \rho_g)\beta}{(\rho_p - \rho_b)}$$

The numerator in our Alpha term contains the breakage component Beta. In an ideal setting with no breakage, the two values should have a one-to-one ratio, but the data shows that Alpha is typically a little greater than the experimentally calculated value. This discrepancy is believed to be caused by uncertainties in the physical characteristics of our materials used in our calculations.

We know that if there are no added beads, the percentage must be zero. If we forced our trend line to begin at the origin, (0,0), we may get closer to a one to one ratio between Alpha and calculated bead percentage, but the data would be less correlated. Even though there are unknown errors in the assumptions of our calculations, looking at a plot of Betas and Alphas in Figure 20, it is clear that Beta will still be a small number.

Note the Axes for Alpha and Beta are very different. Beta remains close to zero while Alpha ranges from about 5% to 55%.

Figure 20.   Alpha versus Beta

The Beta values are only a fraction of the Alpha values. This implies that there is not a significant amount of breakage. Looking at the graph, there are instances of a negative Beta, which is a physical impossibility. It is hypothesized that due to minor errors in measurements and uncertainties in the input constants, namely densities and resistivities of the materials used, the Alpha and Beta values may not be exact. Alpha and Beta are, however, useful for trend analysis and the trend is that there is no significant indication of breakage across the various percentages of glass bubbles to carrier polymer; therefore, to increase the thermal resistivity of our composite material, one should maximize the volumetric percentage of glass bubbles to saturate the carrier polymer.

3. Error Propagation

There are limitations in the precision of our measurements. Much of our data used comes from technical data sheets and other experiments. The three factors believed to be the largest source of error are the density of the intact beads, resistivity of the composite, and density of the composite. 3M gives us a range of .03 $\left(\frac{g}{cm^3}\right)$, which equates to about a 16% error. This stems largely due to the inhomogeneity of the beads. Most of our calculations use the average or typical values of the glass bubbles because when looked at in the macroscopic scale, they should be ideally represented by the average value. In actuality, different sized beads could have different amounts of glass, different densities, and different potential breakage probabilities. It is reasonable to assume larger bubbles would break more readily than the smaller bubbles. This is not taken into account in our calculations.

The material properties of the composite were calculated by Brown to have roughly a 5% uncertainty for both density and resistivity. We will use the following formula to calculate error bars for Alpha:

$$\sigma_{\alpha,Total}^2 = \sigma_{\rho_b}^2 \left(\frac{\delta\alpha}{\delta\rho_b}\right)^2 + \sigma_{\rho_t}^2 \left(\frac{\delta\alpha}{\delta\rho_t}\right)^2 + \sigma_{R_t}^2 \left(\frac{\delta\alpha}{\delta R_t}\right)^2 \tag{27}$$

Beta will be calculated similarly:

$$\sigma_{\beta,Total}^2 = \sigma_{\rho_b}^2 \left(\frac{\delta\beta}{\delta\rho_b}\right)^2 + \sigma_{\rho_t}^2 \left(\frac{\delta\beta}{\delta\rho_t}\right)^2 + \sigma_{R_t}^2 \left(\frac{\delta\beta}{\delta R_t}\right)^2 \tag{28}$$

Once we calculated the error, we can apply the error bars and get Figure 21.
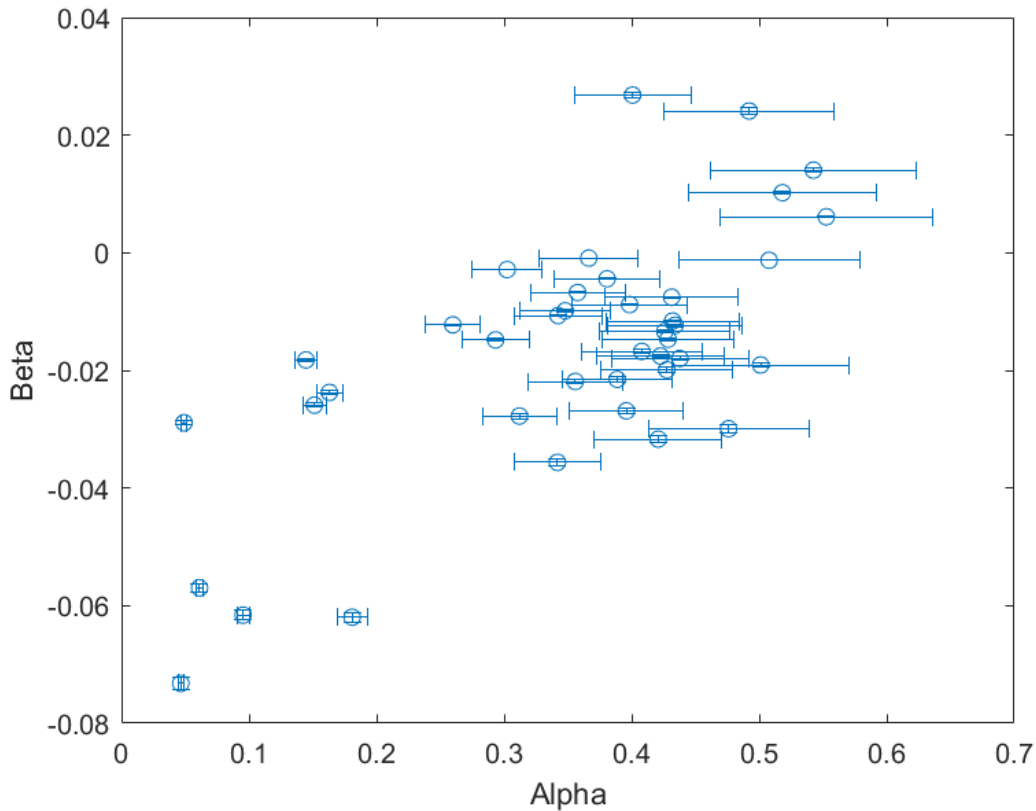
Figure 21.   Alpha versus Beta with Error Bars

Alpha errors ranged from about 4% to 13% depending on the value of Alpha. Beta errors were much tighter, around 1% to 2%. Beta only ranges from about -7% to 3% whereas Alpha ranges from about 5% to 55% so the smaller error bars on Beta is expected.

B.   FUTURE ANALYSIS

1.   Precision

It is believed that many of our errors come from the lack of precision in our data. Many of our densities and conductivities are only known to a couple significant digits. Finding more accurate data could make our simulation a little more representative of the material. Our laboratory recently received a more accurate device to measure resistivities of our composite material. This improvement of accuracy and precision in resistivity measurement could improve our mathematical models.

2.   Glass Bubble Inhomogeneity

As discussed earlier, the glass bubbles we use do not have identical physical properties. The particle size alone range from 30 microns to 120 microns. This diversity of glass bubbles can greatly affect our calculations. Though the density did not have as large of an effect on Alpha and Beta errors as we expected, the particle size can have effects on glass volume, packing density, and resistivity. Different sized particles may have different Betas.

VI. CONCLUSIONS

The COMSOL models revealed that the steric configuration did not matter as much as we initially predicted. The SSSC, BCC, and FCC differed by only a small amount for a given set of material inputs. The material the bubble was modeled as, and therefore the resistivity of the bubble, was the far more significant factor in the resistivity of our component. As expected, pure air produced the most thermally resistive material and the glass-shelled bubble produced the least thermally resistive material. The stated values of thermal conductivity and densities by 3M produced a model that best followed the experimental data gathered by Brown.

One large uncertainty that was not accounted for in our software models was the inhomogeneity of the glass bubbles. Our models simplified the beads to a single size whereas the real glass bubbles range from 30 microns to a maximum size of 120 microns. This can affect both packing volume and shunting effects not fully accounted for in our model. Our model did, however, helped to validate the experimental work done by Brown. The use of the rigid insulation material out performs some of the best neoprene suits in terms of thermal resistance as soon as pressure is applied.

Even though the results of the Alpha and Beta analysis show that there is work left to be done to more accurately model the inner workings of our composite material, both the COMSOL models and the trends that our Alpha and Beta analysis predict reinforce the conclusions that Brown drew from his experiments. The inhomogeneous sizes of the glass bubbles have a large effect on this analysis as well. Larger bubbles may be more prone to breakage than smaller bubbles. Different sized bubbles may also have different volumes of glass than we predicted. Neither effect was taken into account in our Alpha and Beta analysis. However, our work did show a close relationship between our predicted Alphas and Brown's experimental bead percentage. Our Beta values all show that there is a small amount of breakage compared to Alpha. When the material was looked at under the scanning electron microscope in Brown's work, there were no signs of significant breakage [10]. Our Alpha and Beta analysis can be refined in the future to get a more accurate accounting of intact bubble percentage and breakage.

The results of this thesis further show the value of this work. Now that we verified the validity of Brown's work, further research into the flexibility and durability of our composite material can open the doors to a full-sized prototype.

Once the models developed in this thesis are refined, the simulations can be used to optimize the suit. The future models can be used to quickly determine the ideal type of rigid sphere, whether it be a hollow glass sphere or solid ceramic sphere.

This work comes before a critical time for the U.S. Navy. As eyes shift to the north towards the arctic, thermal protection will become more and more relevant.

LIST OF REFERENCES

[1]   Navy Recruiting Command, "Navy diver careers." Accessed 16 July 2018.
        [Online]. Available: https://www.navy.com/careers/navy-diver

[2]   M. G. Hayward and W. R. Keatinge, "Progressive symptomless hypothermia in
        water: Possible cause of diving accidents," *British Medical Journal*, vol. 5, no. 1
        p. 1182, May 5 1979.

[3]   F. L. Beckman, "Thermal protection during immersion in cold water," NMRI,
        Bethesda, MD, USA, Res. Rep. MR 005.13-4001.06, 1964. [Online]. Available:
        http://www.dtic.mil/dtic/tr/fulltext/u2/601044.pdf

[4]   National Oceanic and Atmospheric Administration, *NOAA Diving Manual:
        Diving for Science and Technology, Fourth ed.*, North Palm Beach, FL, USA:
        Best Publishing Company, 2001.

[5]   Naval Sea Systems Command. "U.S. Navy diving manual: Revision 7,"
        December 1, 2016. [Online]. Available:
        http://www.navsea.navy.mil/Portals/103/Documents/SUPSALV/Diving/US%20D
        IVING%20MANUAL_REV7.pdf?ver=2017-01-11-102354-

[6]   Stern Rubber Company, Est. 1969, "Neoprene and polychloroprene," April 2,
        2015. [Online]. Available: https://sternrubber.com/blog/why-you-dont-pee-your-
        neoprene-wet-suit

[7]   Wetsuit Warehouse, "Surf, scuba, spear, and apnea wetties: how do they differ?,"
        September 19, 2017. [Online]. Available:
        https://wetsuitwarehouse.com.au/blogs/news/surf-scuba-spear-and-freediving-
        wetsuits-how-do-they-differ

[8]   Engineering ToolBox, "Specific heat of common substances." Accessed July 17,
        2018. [Online]. Available: https://www.engineeringtoolbox.com/specific-heat-
        capacity-d_391.html

[9]   Engineering ToolBox, "Thermal conductivity of common materials and gases."
        Accessed July 17, 2018. [Online]. Available:
        https://www.engineeringtoolbox.com/thermal-conductivity-d_429.html

[10]   J. M. Brown, "Microsphere-based passive material for low temperature diving
        suits," M.S. thesis, GSEAS, NPS, Monterey, CA, USA, 2018.

[11]   E. Bardy, J. Mollendorf and D. Pendergast, "A comparison of the thermal resistance of a foam neoprene wetsuit to a wetsuit fabricated from aerogel-syntactic foam hybrid insulation," *Journal of Physics D: Applied Physics,* vol. 39, no. 18, pp. 4068–4076, Sep. 2006. [Online]. doi:10.1088/0022-3727/39/18/018

[12]   C. J. M. Lasance, "The thermal conductivity of rubbers/elastomers," Electronics Cooling, November 1, 2001. [Online]. Available: https://www.electronics-cooling.com/2001/11/the-thermal-conductivity-of-rubbers-elastomers/

[13]   E. Algaer, "Thermal conductivity of polymer materials-reverse nonequilibrium molecular dynamics simulation," Ph.D.Dissertation, Dept. of Chemistry, Technishe Universitat Darmstadt, Darmstadt, Germany, 2010. [Online]. Available: http://tuprints.ulb.tu-darmstadt.de/2145/1/Algaer_Dissertation.pdf

[14]   3M, *3M glass bubbles K series, S series, and iM series*, 98-0212-3859-1, 2013. [Online]. Available: https://multimedia.3m.com/mws/media/91049O/3m-glass-bubbles-k-s-and-im-series.pdf

[15]   The Dow Chemical Company, *SYLGARD 184 Silicone Elastomer*, 11-3184B-01, 2017. [Online]. Available: https://www.ellsworth.com/products/by-market/consumer-products/encapsulants/silicone/dow-sylgard-184-silicone-encapsulant-clear-0.5-kg-kit/

[16]   The COMSOL Group, Stockholm, Sweden. 1998. COMSOL Multiphysics, ver. 5.3. [Online]. Available: www.comsol.com

[17]   W. Xiong, "Applications of COMSOL multiphysics software to heat transfer processes," M.S. thesis, Dept. of Industrial Management, Arcada University of Applied Sciences, Helsinki, Finland, 2010. [Online]. Available: https://www.theseus.fi/bitstream/handle/10024/17165/Xiong_Wei.pdf

[18]   P. Berne, "Thermal conductivity of composites: How COMSOL revealed an omission in a classical paper," CEA liten, Grenoble, France, DTNM, SEN, LSN 17 rue des Martyrs, F-38054 Grenoble cedex 9, 2015. [Online]. Available: https://www.comsol.com/paper/thermal-conductivity-of-composites-how-comsol-revealed-an-omission-in-a-classica-23401

[19]   M. F. Ashby, *Materials and the Environment: Eco-informed Material Choice*. Oxford, United Kingdom: Butterworths-Heinemann, 2012.

[20]   Engineering ToolBox, "Air - density, specific weight and thermal expansion coefficient at varying temperature and constant pressures." Accessed July 7, 2018. [Online]. Available: https://www.engineeringtoolbox.com/air-density-specific-weight-d_600.html

[21]   Mayo Clinic. "Hypothermia—symptoms and causes." Accessed July 16, 2018. [Online]. Available: https://www.mayoclinic.org/diseases-conditions/hypothermia/symptoms-causes/syc-20352682

[22]   Glenn Research Center, "Boyle's law," National Aeronautics and Space Administration, May 5, 2015. [Online]. Available: https://www.grc.nasa.gov/WWW/k-12/airplane/boyle.html

THIS PAGE INTENTIONALLY LEFT BLANK

INITIAL DISTRIBUTION LIST

1.   Defense Technical Information Center
        Ft. Belvoir, Virginia

2.   Dudley Knox Library
        Naval Postgraduate School
        Monterey, California